The Astrophysical Journal, 651:392–400, 2006 November 1

INTERACTION OF MASSIVE BLACK HOLE BINARIES WITH THEIR STELLAR ENVIRONMENT. I. EJECTION OF HYPERVELOCITY STARS

Alberto Sesana,[1] Francesco Haardt,[1] and Piero Madau[2]
Received 2006 April 13; accepted 2006 July 8

ABSTRACT

We use full three-body scattering experiments to study the ejection of hypervelocity stars (HVSs) by massive black hole binaries (MBHBs) at the centers of galaxies. Ambient stars drawn from a Maxwellian distribution unbound to the binary are expelled by the gravitational slingshot. Accurate measurements of thermally averaged hardening, mass ejection, and eccentricity growth rates (H, J, and K) for MBHBs in a fixed stellar background are obtained by numerical orbit integration from initial conditions determined by Monte Carlo techniques. Three-body interactions create a subpopulation of HVSs on nearly radial orbits, with a spatial distribution that is initially highly flattened in the inspiral plane of the MBHB, but becomes more isotropic with decreasing binary separation. The degree of anisotropy is smaller for unequal mass binaries and larger for stars with higher kick velocities. Eccentric MBHBs produce a more prominent tail of high-velocity stars and break planar symmetry, ejecting HVSs along a broad jet perpendicular to the semimajor axis. The jet two-sidedness decreases with increasing binary mass ratio, while the jet opening angle increases with decreasing kick velocity and orbital separation. The detection of a numerous population of HVSs in the halo of the Milky Way by the next generation of large astrometric surveys such as *Gaia* may provide a unique signature of the history, nature, and environment of the MBH at the Galactic center.

Subject headings: black hole physics — methods: numerical — stellar dynamics

1. INTRODUCTION

Massive black holes (MBHs) are a ubiquitous component of nearby galaxy nuclei (e.g., Magorrian et al. 1998), and galaxies experience multiple hierarchical mergers during their lifetime. Following the merger of two halo+MBH systems of comparable mass ("major mergers"), dynamical friction is known to effectively drag in the satellite halo (and its MBH) toward the center of the more massive progenitor; this will lead to the formation of a bound MBH binary (MBHB) in the violently relaxed core of the newly merged stellar system (Begelman et al. 1980). Even in the case of unequal-mass mergers, gas cooling appears to facilitate the pairing process by increasing the resilience of the companion galaxy to tidal disruption (Kazantzidis et al. 2005). It is expected then that many galaxies will host wide MBHBs during cosmic history (e.g., Volonteri et al. 2003). As the binary separation decays, the effectiveness of dynamical friction slowly declines because distant stars perturb the binary's center of mass but not its semimajor axis. The bound pair then loses orbital energy by capturing stars passing in its immediate vicinity and ejecting them at much higher velocities ("gravitational slingshot").

It was first pointed out by Hills (1988) that the tidal breakup of binary stars by a MBH at the Galactic center may eject one member of the binary with velocities $\sim$1000 km s^{-1}. Such "hypervelocity stars" (HVSs) are also produced by three-body interactions between ambient stars with low angular momentum orbits and a "hard" MBHB, i.e., a binary whose binding energy per unit mass exceeds the star specific kinetic energy. Assuming Sgr A* to be one component of a MBHB, Yu & Tremaine (2003) estimated the number of HVSs expected within the solar radius to be $\sim 10^3$. Brown et al. (2005) reported the first discovery of a HVS (with a Galactic rest-frame velocity in excess of 700 km s^{-1}) in the Galactic halo. This and five more HVSs, recently discovered by Hirsch et al. (2005) and Brown et al. (2006a, 2006b), are all consistent with a Galactic center origin, while an ejection from the LMC is more plausible for the seventh HVS currently known (Edelmann et al. 2005). Holley-Bockelmann et al. (2005) have proposed that the anomalously fast intracluster planetary nebulae identified in the Virgo Cluster by Arnaboldi et al. (2004) may also be associated with close three-body interactions with a MBHB at the center of M87. Unbound HVSs travel with velocities so extreme that dynamical ejection from a relativistic potential is the most plausible origin, and they are becoming increasingly recognized as an important tool for understanding the history, nature, and environment of nuclear MBHs.

Stars expelled by a MBHB are expected to form a subpopulation with very distinct kinematics (e.g., Quinlan 1996, hereafter Q96), as well as spatial structure (Zier & Biermann 2001). The phase-space distribution of HVSs ejected by an intermediate-mass black hole (IMBH) inspiralling into Sgr A* has been recently studied analytically by Levin (2005). Stars bound to Sgr A* and drawn from an isotropic cusp are ejected in a burst lasting a few dynamical friction timescales; most stars are expelled isotropically if the inspiral is circular, or in a broad "jet" aligned with the IMBH velocity at pericenter if the inspiral is eccentric (Levin 2005). Yet most HVSs are produced during the phases of the inspiral that cannot be modeled analytically. This is the first paper in a series aimed at a detailed numerical study of the interaction of MBHBs with their dense stellar environment. We use here full three-body scattering experiments of the ejection of background stars by MBHBs at the center of galaxies to address the kinematic properties of HVSs. Ambient stars drawn from a Maxwellian distribution unbound to the binary are expelled by the gravitational slingshot. Reaction rates are obtained by numerical orbit integration from initial conditions determined by Monte Carlo techniques. The plan of the paper is as follows. In § 2, we describe our suite of three-body scattering experiments. In § 3, we present accurate measurements of the binary hardening, mass ejection, and eccentricity growth rates for MBHBs embedded in a fixed stellar background, reproducing Q96's classical

[1] Dipartimento di Fisica e Matematica, Universitá dell'Insubria, via Valleggio 11, 22100 Como, Italy.
[2] Department of Astronomy and Astrophysics, University of California, 1156 High Street, Santa Cruz, CA 95064.

results. In § 4, we discuss the detailed kinematic properties of the ejected subpopulation. Finally, we present our conclusions in § 5.

2. SCATTERING EXPERIMENTS

Consider a binary of mass $M = M_1 + M_2$ ($M_2 \leq M_1$), reduced mass $\mu = M_1 M_2/M$, and semimajor axis a, orbiting in the x-y plane in a background of stars of mass m_*. In the case of a light intruder with $m_* \ll M_2$, the problem is greatly simplified by setting the center of mass of the binary at rest at the origin of the coordinate system. It is then convenient to define an approximated dimensionless energy change C and angular momentum change B in a single binary-star interaction as (Hills 1983)

$$C = \frac{M}{2m_*}\frac{\Delta E}{E} = \frac{a\Delta E_*}{G\mu}, \tag{1}$$

and

$$B = -\frac{M}{m_*}\frac{\Delta L_z}{L_z} = \frac{M}{\mu}\frac{\Delta L_{z*}}{L_z}, \tag{2}$$

where $\Delta E/E$ is the fractional increase (decrease if negative) in the orbital specific binding energy $E = -GM/(2a)$, $\Delta L_z/L_z$ is the fractional change in orbital specific angular momentum $L_z = [GMa(1-e^2)]^{1/2}$, and ΔE_* and ΔL_{z*} are the corresponding changes for the interacting star. Conservation of total energy and angular momentum lead to the following expression for the change in orbital eccentricity e,

$$\Delta e = \frac{(1-e^2)}{2e}\frac{2m_*}{M}(B - C). \tag{3}$$

The quantities B and C are of order unity and are derived by three-body scattering experiments that treat the star-binary encounters one at a time (Hut & Bahcall 1983; Q96). For each encounter one solves nine coupled, second-order differential equations,

$$\ddot{\boldsymbol{r}}_i = -G\sum_{i\neq j}\frac{m_j(\boldsymbol{r}_i - \boldsymbol{r}_j)}{|\boldsymbol{r}_i - \boldsymbol{r}_j|^3}, \tag{4}$$

supplied by 18 initial conditions $\boldsymbol{r}_i(t=0)$, $\dot{\boldsymbol{r}}_i(t=0)$. The incoming star is moved from $r = \infty$ to $r_i = (10^{10}\mu/M)^{1/4}a$ on a Keplerian orbit about a point mass M. At r_i, the force induced by the quadrupole moment of the binary is 10 orders of magnitude smaller than the total force acting on the star at a distance a, and numerical integration starts. The initial conditions define a point in a nine-dimensional parameter space given by

1. The mass ratio $q = M_2/M_1$ of the binary.
2. The eccentricity of the binary e.
3. The mass of the star m_*.
4. The asymptotic initial speed of the incoming field star $v \equiv |\boldsymbol{v}|$.
5. The impact parameter at infinity b (the distance at which the star would pass the binary if it fell no attraction).
6. Four angles: θ and ϕ describing the initial direction of the impact, ψ its initial orientation, and Ψ the initial binary phase.

A significant star-binary energy exchange (i.e., characterized by a dimensionless energy change $C > 1$) occurs only for $v/V_c < (M_2/M)^{1/2}$, where $V_c = (GM/a)^{1/2}$ is the binary orbital velocity (the relative velocity of the two holes if the binary is circular, see, e.g., Saslaw et al. 1974; Mikkola & Valtonen 1992). We sample this quantity in the range $3\times10^{-3}(M_2/M)^{1/2} < v/V_c < 30(M_2/M)^{1/2}$ with 80 logarithmically equally spaced grid points. Note that varying the incoming velocity at a fixed V_c is equivalent to varying the binary separation a at a fixed v. When averaged over a Maxwellian distribution, the range of v/V_c sampled in our experiments therefore probes the slingshot mechanism over about four decades in binary separation.

Each scattering experiment requires five random numbers. The impact parameter is related to the star pericenter distance r_p by

$$b^2 = r_p^2\left(1 + \frac{2GM}{r_p v^2}\right). \tag{5}$$

For each incoming velocity the impact parameter is randomly sampled according to an equal probability distribution in b^2 (equivalent to a probability weight proportional to b), in an interval corresponding to a range in scaled pericenter distance r_p/a of $[0, 5]$. In a number of test cases, we have extended this range to $[0, 10]$, finding little differences in the measured hardening rates. The velocity angles θ and ϕ are randomly generated to reproduce a uniform density distribution over a spherical surface centered in the origin of coordinate system, while the orientation angle ψ is chosen from a uniform distribution in the range $[0, 2\pi]$. The probability distribution of the binary phase Ψ is sampled by weighting randomly selected angles according to the time spent by the binary in any given phase range. Given a set of initial conditions, we integrate the system of differential equations (eq. [4]) using the most recent version of the subroutine DOPRI5,[3] which is based on an explicit Runge-Kutta method of order 4(5) due to Dormand & Prince (1978). A complete description of the integrator can be found in Hairer et al. (1993).

As the total energy of the binary star system is always negative, a bound triple system may form temporarily, but will typically dissolve within 10–100 crossing times (Valtonen & Aarseth 1977). The integration is stopped if one of the following events occurs: (*a*) the star leaves the sphere of radius r_i with positive total energy; (*b*) the integration reaches 10^6 time steps (corresponding to between a few hundred and a thousand binary orbital periods); or (*c*) the physical integration time exceeds 10^{10} yr. The integration of the full three-body problem allows us to directly control the conservation of total energy and angular momentum. The code adjusts the integration step size to keep the fractional error per step, ϵ, in the position and velocity below a level that was set to 10^{-11}. This allows a total energy conservation accuracy $\Delta E/E \sim 10^{-9}$ in a single orbit integration, while, for $m_*/M \simeq 10^{-7}$, the star energy is conserved, in a single orbit, at level of one part in a hundred. We have also checked that our choice of erasing from the record stars that get captured for long times does not affect results appreciably. Abandoned integrations involve, for the major part, encounters with stars that get captured in very weakly bound orbits (energetically "poor" events) and make many revolutions before being expelled. The fraction of erased stars that are instead captured in tightly bound orbits (hence energetically "rich") is quite small, $\lesssim 10^{-4}$, assuring that the global impact of such encounters on the evolution of binary orbital parameters is indeed negligible.

We have performed 24 sets of scattering experiments for binary mass ratios $q = 1$, 1/3, 1/9, 1/27, 1/81, and 1/243, and initial eccentricities $e = 0.01$, 0.3, 0.6, and 0.9. After each orbit integration the x, y, z components of $\boldsymbol{v}$ and $\boldsymbol{L}$ are stored. Each run involves 4×10^6 stars; we collect partial outputs after 5×10^4

[3] See http://www.unige.ch/math/folks/hairer/software.html.

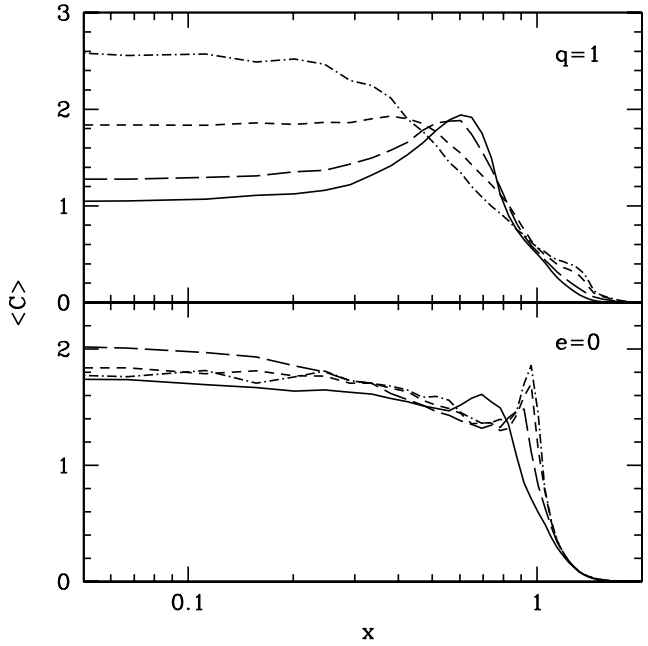

FIG. 1.—*Top:* Mean energy exchange $\langle C\rangle$ as a function of dimensionless impact parameter x for an equal-mass binary with eccentricity $e = 0$ (*solid line*), 0.3 (*long-dashed line*), 0.6 (*short-dashed line*), and 0.9 (*dot-dashed line*). *Bottom:* Same, but for a circular binary with mass ratio $q = 1/3$ (*solid line*), 1/9 (*long-dashed line*), 1/27 (*short-dashed line*), and 1/81 (*dot-dashed line*).

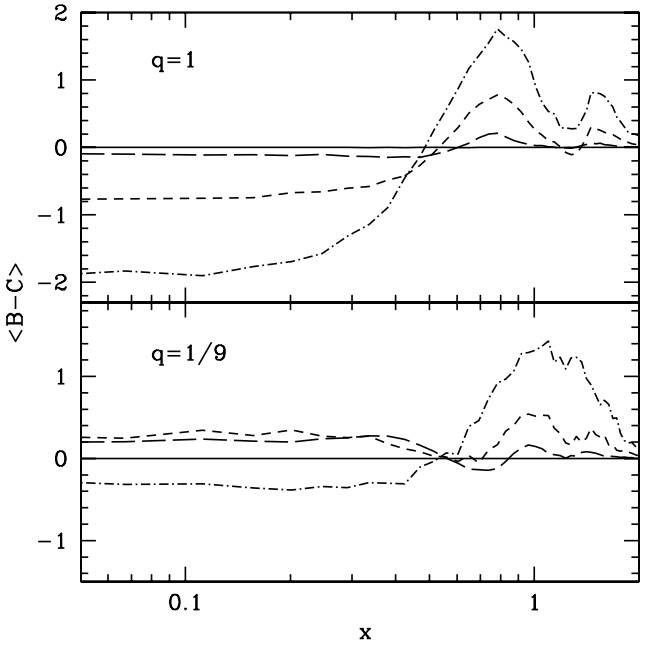

FIG. 2.—Mean angular momentum minus energy exchange $\langle B - C\rangle$ parameter as a function of dimensionless impact parameter x for a binary with eccentricity $e = 0$ (*solid line*), 0.3 (*long-dashed line*), 0.6 (*short-dashed line*), and 0.9 (*dot-dashed line*). *Top:* Equal-mass binary ($q = 1$). *Bottom:* $q = 1/9$.

orbit integrations corresponding to a given initial speed v, calculate the values of $\langle C\rangle$ and $\langle B\rangle$ averaged over orbital angular variables, and then evaluate the hardening, eccentricity growth, and mass ejection rates as defined in the § 3. Statistical errors are estimated by evaluating the rates from 10 different orbit subsets, and then computing standard deviations (see § 3).

Figure 1 shows examples of the energy exchange parameter $\langle C\rangle$ versus the star impact parameter b in the limit $v \ll V_c$, i.e., for a "hard" binary. We have defined a rescaled dimensionless impact parameter x as in Q96 as

$$x \equiv b/b_0, \quad b_0^2 = 2GMa/v^2, \tag{6}$$

where b_0 is the impact parameter at infinity leading to a star pericenter $r_p = a$ including gravitational focusing. For a circular, equal-mass binary, $\langle C\rangle$ has a maximum for impact parameter equal to the distance of each binary member from the center of mass ($x \simeq 0.5$), and then decreases reaching a constant value $\langle C\rangle \simeq 1$ for small impact parameters. In the case of highly eccentric binaries ($e = 0.9$), the energy exchange is almost monotonic; a star with small impact parameter interacts with the pair near pericenter when it has maximum speed, and this results in a large energy exchange. For circular binaries and $x \lesssim 1$, one finds $1.5 \lesssim \langle C\rangle \lesssim 2$ nearly independently of the mass ratio. The peak at $x = 1$ for $q \ll 1$ corresponds to the location of M_2, as M_1 is now at rest and M_2 orbits around M_1 at distance a. From equation (1) it follows that stars typically experience an energy gain proportional to the reduced mass of the binary, and inversely proportional to the binary separation. The combination $\langle B(x) - C(x)\rangle$, which governs the eccentricity evolution (see eq. [12]), is shown in Figure 2. For a circular binary $\langle B - C\rangle$ is zero independently of impact parameter, i.e., circular binaries remain circular. If the binary is eccentric, $\langle B - C\rangle$ shows a positive peak for impact parameters corresponding to close encounters with M_2 or with one member of an equal-mass pair. Interactions with $0.5 \lesssim x \lesssim 2$ stars tend to increase the eccentricity of the binary, whereas stars with low impact parameter have either a small effect ($q = 1/9$) or can significantly decrease the eccentricity ($q = 1$). Typically, $B \propto \Delta L_{z*}$ assumes positive values, i.e., scattered stars gain angular momentum along the z-axis and will tend to corotate with the binary.

3. HARDENING IN A FIXED BACKGROUND

As described in Q96, the binary evolution in an isotropic fixed background of stars of density ρ and one-dimensional velocity dispersion σ at infinity is determined by three dimensionless quantities: the hardening rate

$$H = \frac{\sigma}{G\rho}\frac{d}{dt}\left(\frac{1}{a}\right), \tag{7}$$

the mass ejection rate ($M_{\rm ej}$ is the stellar mass ejected by the binary)

$$J = \frac{1}{M}\frac{dM_{\rm ej}}{d\ln(1/a)}, \tag{8}$$

and the eccentricity growth rate

$$K = \frac{de}{d\ln(1/a)}. \tag{9}$$

The average hardening rate for a Maxwellian stellar velocity distribution $f(v,\sigma) = (2\pi\sigma^2)^{-3/2}\exp(-v^2/2\sigma^2)$ is

$$H(\sigma) \equiv \int_0^\infty f(v,\sigma)\frac{\sigma}{v}H_1(v)4\pi v^2\,dv, \tag{10}$$

where

$$H_1(v) \equiv 8\pi\int_0^\infty \langle C\rangle x\,dx \tag{11}$$

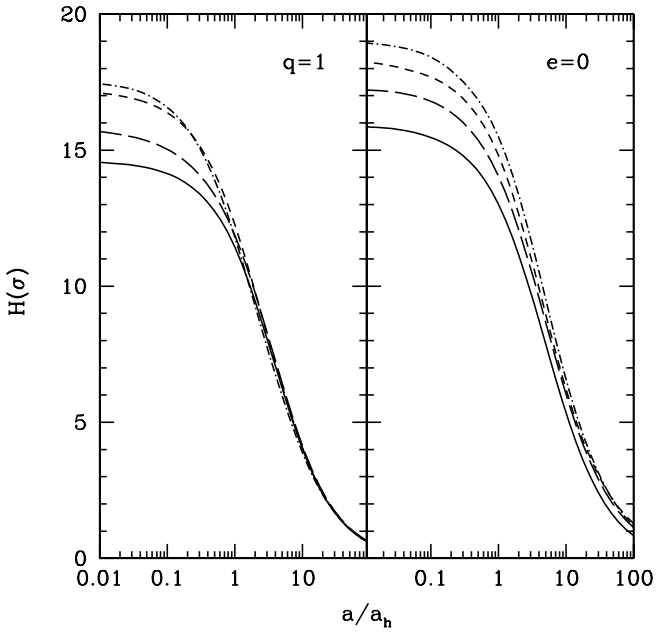

FIG. 3.—Binary hardening rate H (averaged over a Maxwellian velocity distribution) vs. a/a_h. *Left:* $e = 0, 0.3, 0.6$, and 0.9 for $q = 1$. *Right:* $q = 1/3, 1/9, 1/27$, and 1/81 for $e = 0$. Line style as in Fig. 1.

is the dimensionless hardening rate if all stars have the same velocity v. An expression analogous to equation (10) relates the thermally averaged eccentricity growth rate $K(\sigma)$ to $K_1(v)$, where

$$K_1(v) \equiv \frac{(1-e^2)}{2e}\frac{\int_0^\infty \langle B - C\rangle x\, dx}{\int_0^\infty \langle C\rangle x\, dx}. \quad (12)$$

Both H_1 and K_1 are independent of M and m_*. Figure 3 shows the hardening rate H versus binary separation a as derived from our scattering experiments. As found by Q96, H is approximately constant for

$$a < a_h = \frac{GM_2}{4\sigma^2}. \quad (13)$$

Defining as "hard" a binary whose orbital separation is smaller than a_h, it follows then that a "hard" binary hardens at a constant rate. Note that there is no explicit dependence on σ once the rate is expressed as a function of a/a_h. The value of H is found to be a decreasing function of q but increases with increasing eccentricity. The latter trend can be understood from Figure 1, which shows a significative enhancement in the energy change $\langle C\rangle$ at small impact parameters at increasing eccentricity. Note that H drops to zero for $a \gtrsim 10a_h$. We choose the following ejection criterion to measure the rate at which the binary ejects stars. The binary is assumed to be embedded in a bulge of mass M_B and stellar density profile approximated by a singular isothermal sphere (SIS). Stars are counted as "ejected" from the bulge if, after three-body scattering, their velocity V far away from the binary is greater than the escape velocity from the radius of influence of the binary, $r_{\rm inf} \equiv GM/(2\sigma^2)$. The SIS potential is $\phi(r) = -2\sigma^2[\ln(GM_B/2\sigma^2 r) + 1]$ (for $r < R_B = GM_B/2\sigma^2$), and the escape speed from $r_{\rm inf}$ is then

$$v_{\rm esc} \equiv \sqrt{-2\phi} = 2\sigma\sqrt{\ln(M_B/M) + 1} = 5.5\sigma, \quad (14)$$

where the second equality comes from the adopted bulge–black hole mass relation $M = 0.0014M_B$ (Haring & Rix 2004). Note that this yields a more conservative ejection criterion than the conventional choice $V > v_{\rm esc} = 2\sqrt{3}\sigma$ adopted by Q96.[4] Denoting with $F_{\rm ej}(x, v, \sigma)$ the fraction of incident stars with impact parameter x and initial velocity v that satisfy equation (14) after a three-body interaction, the thermally averaged ejection rate can then be written as

$$J(\sigma) \equiv \frac{1}{H}\int_0^\infty f(v,\sigma)\frac{\sigma}{v}4\pi v^2\, dv\; 4\pi\int_0^\infty F_{\rm ej}\, x\, dx. \quad (15)$$

We have found that the (Maxwellian averaged) rates H, J, and K derived from scattering experiments can be fitted to within few percent by the following functions:

$$H = A(1 + a/a_0)^\gamma, \quad (16)$$

$$J = A(a/a_0)^\alpha[1 + (a/a_0)^\beta]^\gamma, \quad (17)$$

and

$$K = A(1 + a/a_0)^\gamma + B. \quad (18)$$

The parameters of the fits to H and J are listed in Tables 1 and 2 for different binary mass ratios and circular orbits, while fit parameters to K are listed in Table 3 for different values of q and e. The binary eccentricity growth and mass ejection rates K and J (averaged over a Maxwellian distribution) are plotted in Figures 4 and 5 as a function of a/a_h. The parameter K is close to

TABLE 1
HARDENING RATE

q	A	a_0	γ
1	14.55	3.48	−0.95
1/3	15.82	4.18	−0.90
1/9	17.17	3.59	−0.79
1/27	18.15	3.32	−0.77
1/81	18.81	3.87	−0.82
1/243	19.16	4.16	−0.86

NOTES.—Best-fit parameters describing (see eq. [16]) the hardening rate H for a circular binary with varying mass ratio q. The parameter a_0 is given in units of a_h.

[4] When the binary first becomes hard, only a few stars acquire a kick velocity large enough to escape the host bulge. Many scattered stars will instead return to the central region on nearly unperturbed, small-impact parameter orbits, and will undergo a second superelastic scattering with the binary. We will quantify the role of these "secondary slingshots" in determining the hardening of the pair in a subsequent work.

TABLE 2
MASS EJECTION RATE

q	A	a_0	γ	α	β
1	0.224	1.741	−10.986	−0.165	1.095
1/3	0.201	1.784	−7.360	−0.185	1.176
1/9	0.214	0.803	−2.738	−0.200	1.291
1/27	0.215	0.565	−1.853	−0.207	1.374
1/81	0.211	0.424	−1.319	−0.220	1.564
1/243	0.210	0.389	−1.210	−0.222	1.638

NOTES.—Best-fit parameters describing (see eq. [17]) the mass ejection rate J for a circular binary with varying mass ratio. The parameter a_0 is given in units of a_h.

TABLE 3
Eccentricity Growth Rate

e	A	a_0	γ	B
		$q = 1$		
0.15	0.037	0.339	−3.335	−0.012
0.3	0.075	0.151	−1.548	−0.008
0.45	0.105	0.088	−0.893	−0.005
0.6	0.121	0.090	−0.895	−0.008
0.75	0.134	0.064	−0.544	−0.006
0.9	0.082	0.085	−0.663	−0.004
		$q = 1/3$		
0.15	0.082	0.042	−0.168	−0.048
0.3	0.095	0.213	−1.152	−0.012
0.45	0.129	0.137	−0.655	−0.006
0.6	0.166	0.081	−0.546	−0.006
0.75	0.159	0.079	−0.497	−0.010
0.9	0.095	0.122	−0.716	−0.008
		$q = 1/9$		
0.15	0.051	0.385	−0.891	−0.011
0.3	0.111	0.307	−1.107	−0.007
0.45	0.172	0.526	−1.174	−0.016
0.6	0.181	0.251	−1.169	−0.007
0.75	0.179	0.195	−0.846	−0.004
0.9	0.117	0.400	−1.170	−0.001
		$q = 1/27$		
0.15	0.064	0.284	−1.206	0.021
0.3	0.143	1.033	−1.537	−0.021
0.45	0.212	0.722	−1.257	−0.022
0.6	0.216	0.430	−1.163	−0.014
0.75	0.173	0.771	−1.934	−0.014
0.9	0.129	0.329	−1.125	−0.020

Notes.—Best-fit parameters describing (see eq. [18]) the eccentricity growth rate K for varying initial eccentricity e and mass ratio q. The parameter a_0 is given in units of a_h.

zero for $a \sim a_h$, and grows monotonically in the case of eccentric orbits as the binary shrinks. Smaller values of q lead to larger growth rates. In the circular case K is negligible at every separation, i.e., circular binaries remain circular. The mass ejection rate has only a weak dependence on eccentricity and mass ratio.

It is interesting to compare our fits to those provided by Q96. While our results for the dimensionless rates H_1 and K_1 are consistent with those of Q96, within the statistical errors, we have directly fit the Maxwellian-averaged rates for ease of use. Our choice of a different velocity threshold for ejection makes our mass ejection rate $J(\sigma)$ generally lower than that of Q96. Regarding $H(\sigma)$, limiting values for small separations are virtually identical to those of Q96, while at $a \sim a_h$ the fit in Q96 is 20% above our formula. As for the eccentricity growth rate, we have covered a much wider region of the (q, e) parameter space, compared to the limited sampling provided by Q96.

4. KINEMATICS OF HYPERVELOCITY STARS

When the MBHB separation is $a \lesssim a_h$, only a small fraction ($\lesssim$1%) of bulge stars have low angular momentum trajectories with pericenters lying within a (the binary's geometrical "loss cone"). If the loss cone is constantly refilled as the pair shrinks, then a substantial subpopulation of suprathermal HVSs will be produced via the gravitational slingshot. In this section we use

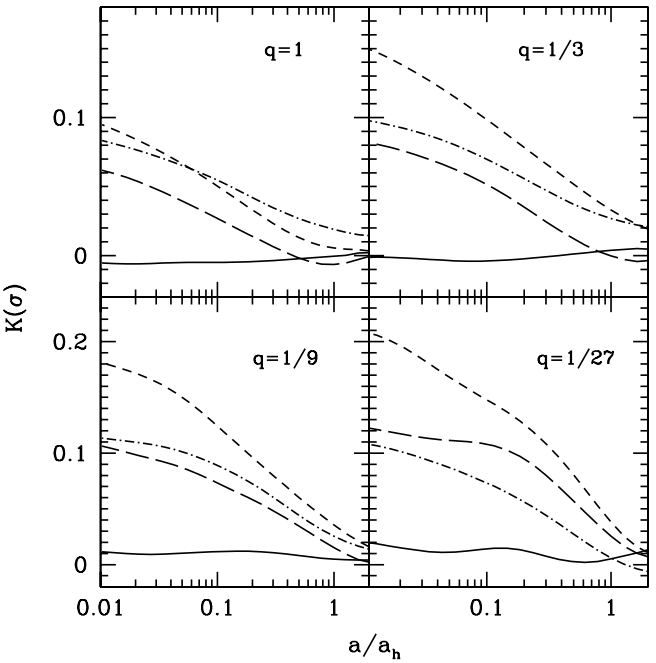

Fig. 4.—Binary eccentricity growth rates as a function of binary separation for different mass ratios. Different line styles are for $e = 0$, 0.3, 0.6, and 0.9, as in the top panel of Fig. 1.

our scattering experiments to study the kinematic of HVSs as a function of binary mass ratio, eccentricity, and orbital separation.

4.1. *Velocity Distribution*

In a scattering event, a star that starts with a low initial velocity v passes the two MBHs at a distance $\sim a$ and leaves with a gain to its kinetic energy, $V^2 \simeq 2C(\mu/M)V_c^2 = [8C\sigma^2/(1+q)](a_h/a)$ (eq. [1]), where C depends on the impact parameter (see Fig. 1). Figure 6 shows the average final velocity of scattered stars $\langle V \rangle$ as a function of inverse binary separation, for different mass

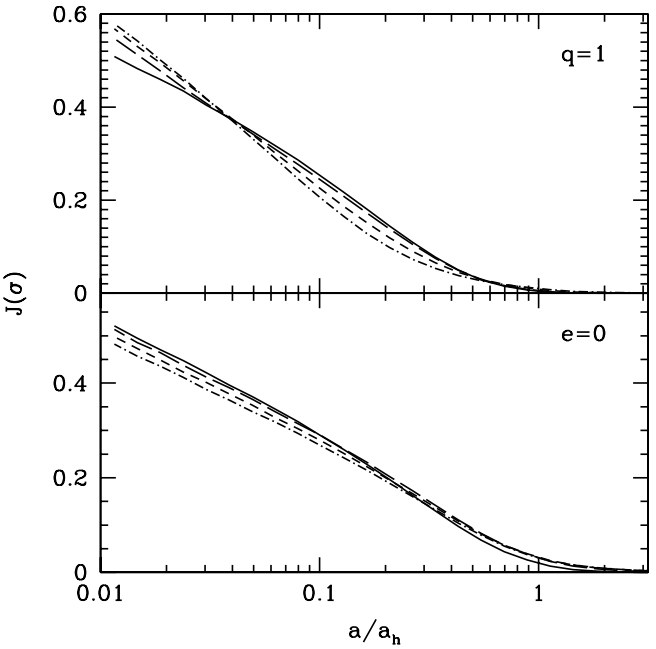

Fig. 5.—Mass ejection rate J vs. a/a_h. *Top:* $e = 0$, 0.3, 0.6, and 0.9 for $q = 1$. *Bottom:* $q = 1/3$, 1/9, 1/27, and 1/81 for $e = 0$. Line style as in Fig. 1.

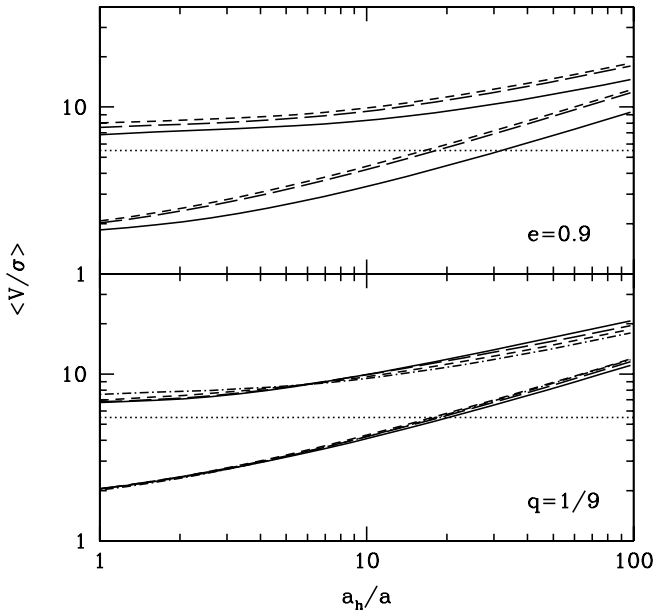

FIG. 6.—Average final velocity $\langle V \rangle$ of all scattered stars vs. inverse binary separation a_h/a. *Top:* Eccentric $e = 0.9$ binary with $q = 1$ (*solid lines*), $q = 1/9$ (*long-dashed lines*), and $q = 1/81$ (*short-dashed lines*). The lower set of curves shows results for the entire population of scattered stars (defined as those with impact parameter at infinity $x \leq 2$), while the upper set of curves shows only HVSs with $V > v_{\rm esc} = 5.5\sigma$. The dotted line in both panels marks the value $V = v_{\rm esc}$. *Bottom:* Same but for $q = 1/9$ binary with $e = 0$ (*solid lines*), $e = 0.3$ (*long-dashed lines*), $e = 0.6$ (*short-dashed lines*), and $e = 0.9$ (*dot-dashed lines*).

ratios and eccentricities. The population includes all stars with maximum impact parameter at infinity $x \leq 2$, corresponding to a pericenter $r_p \leq 4a$. The curves clearly follow the expected $V \propto (a_h/a)^{1/2}$ scaling. For $a_h/a \gtrsim 10$, most scattering events produce HVSs that escape from the bulge. Neither the binary mass ratio nor its eccentricity have a large effect on the average final velocity. Larger eccentricities produce a more prominent high-velocity tail of HVSs, as in this case the orbital velocity of M_2 close to pericenter is larger than V_c, allowing for more energetic slingshots. Our numerical experiments show that both a small mass ratio and a large eccentricity tend to increase the fraction of extremely energetic scattering events.

TABLE 4
VELOCITY DISTRIBUTION

e	A	α	β	γ
0	0.236	−0.917	16.365	−0.165
0.3	0.242	−1.067	11.722	−0.235
0.6	0.385	−0.765	4.627	−0.726
0.9	0.556	−0.599	2.375	−1.420

NOTE.—Best-fit parameters describing (see eq. [19]) the velocity distribution of scattered stars with $4\sigma \lesssim V \lesssim 3V_{\rm max}$.

The properties of scattered stars are best described by noticing that, when stellar ejection velocities are measured in units of binary orbital velocity V_c, the high-velocity tail of the resulting distribution function is actually scale-invariant, i.e., independent of binary separation for fixed q and e. This is clearly shown in Figure 7. Scale invariance is broken by the choice of an absolute velocity threshold (e.g., $V > v_{\rm esc}$) that, in units of V_c, is a decreasing function of a_h/a. The high-velocity tail of the distribution function of scattered stars can be described as a broken power law in the range $4\sigma \lesssim V \lesssim 3V_{\rm max}$, where $V_{\rm max} = V_c[(1+e)/(1-e)]^{1/2}/(1+q)$ is the velocity of the lighter black hole at the pericenter:

$$f(w) = \frac{A}{h}\left(\frac{w}{h}\right)^{\alpha}\left[1+\left(\frac{w}{h}\right)^{\beta}\right]^{\gamma}, \qquad (19)$$

where $w \equiv V/V_c$, and $h \equiv (2q)^{1/2}/(1+q)$. Best-fitting parameters are given in Table 4 for different values of the eccentricity, while the fitting formula and the scattering experiment data are compared in Figure 8. The velocity distribution of HVSs

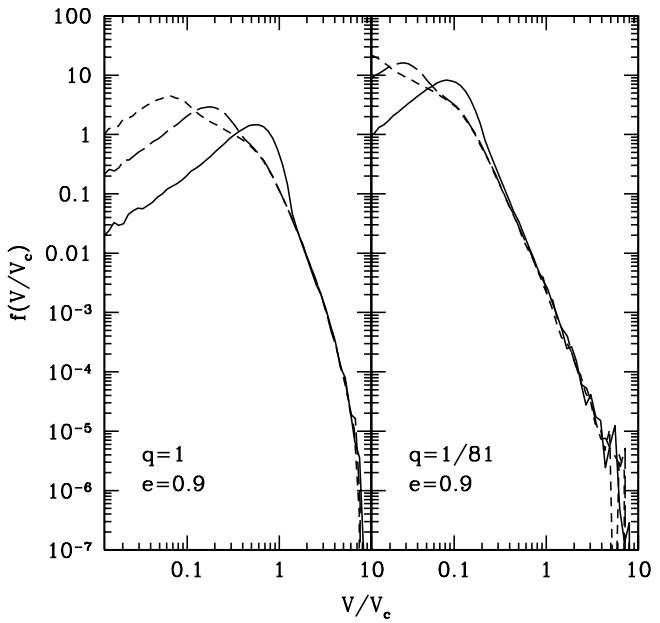

FIG. 7.—Differential distribution of V/V_c for all stars scattered at binary separation $a_h/a = 1$ (*solid line*), 10 (*long-dashed line*), and 100 (*short-dashed line*). As the binary shrinks, the peak shifts to increasingly small values of V/V_c, since injected stars are drawn from a thermal distribution of fixed velocity dispersion σ. *Left:* Binary with $q = 1$ and $e = 0.9$. *Right:* Binary with $q = 1/81$ and $e = 0.9$.

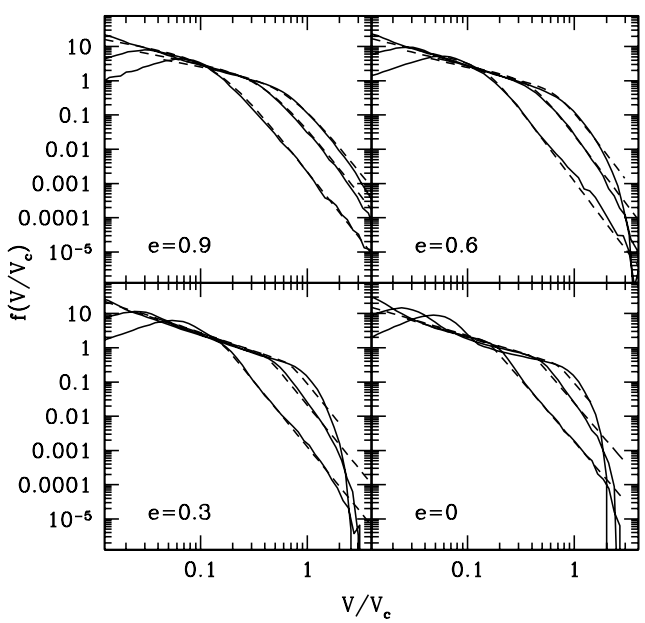

FIG. 8.—Differential distribution of V/V_c for all stars scattered at binary separation $a_h/a = 100$. In each panel values are shown, right to left, for binary mass ratios $q = 1$, 1/9, and 1/81. Scattering experiment data are shown as solid lines, while fitting formula results, extended up to $V = 3V_{\rm max}$ (eq. [19], and Table 4), as dashed lines. The appropriate values of the eccentricity are labeled in each panel.

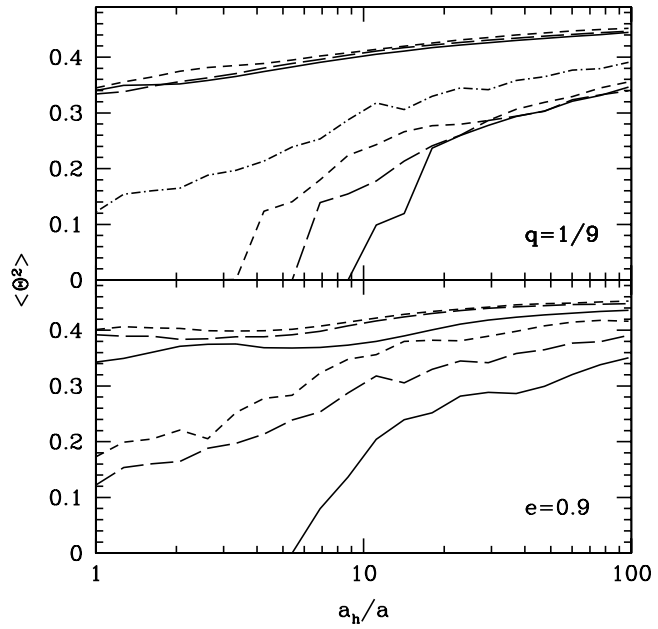

FIG. 9.—Mean value of θ^2 vs. a_h/a for HVSs, where θ is the latitude angle between the star velocity vector at infinity and the binary orbital plane. In each panel, the upper set of curves refers to all ejected stars ($V > v_{esc}$), the lower set of curves to stars with $V > 9v_{esc}$. *Top:* Binary with mass ratio $q = 1/9$ and eccentricity $e = 0$ (*solid lines*), $e = 0.3$ (*long-dashed lines*), $e = 0.6$ (*short-dashed lines*), and $e = 0.9$ (*dot-dashed lines*). *Bottom:* Eccentric binary with $e = 0.9$ mass ratio $q = 1$ (*solid lines*), $q = 1/9$, (*long-dashed lines*), and $q = 1/81$ (*short-dashed lines*).

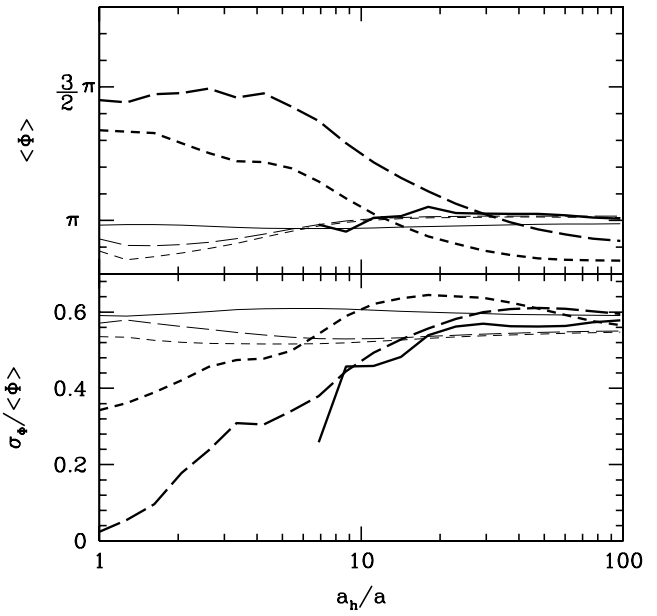

FIG. 10.—*Top:* Mean longitude $\langle\phi\rangle$ of ejected stars as a function of orbital separation. The binary semimajor axis lies along the x-vector, the MBHs orbit counterclockwise in the x-y plane, and the binary eccentricity is set to 0.9. The solid, short-dashed, and long-dashed curves show values for $q = 1$, 1/9, and 1/81, respectively. *Thin lines:* Entire population of ejected stars ($V > v_{esc}$). *Thick lines:* Subset of HVSs with $V > 9\ v_{esc}$. *Bottom:* Relative azimuthal dispersion $\sigma_\phi/\langle\phi\rangle$.

($V > v_{esc}$) at a given binary separation is related to the mass ejection rate by

$$J(a) = -\frac{d(M_{ej}/M)}{da/a} = \int_{v_{esc}/V_c}^{\infty} f(w)\, dw. \qquad (20)$$

Equation (20) sets the normalization constant A in equation (19).

4.2. *Angular Distribution*

Analytic expressions for the time-dependent phase-space distribution of stars ejected from the Galactic center as a result of inspiral of an intermediate-mass black hole ($q \ll 1$) have been recently derived by Levin (2005). HVSs are found to follow a characteristic angular pattern: (1) they are ejected preferentially in the orbital plane of the MBHB, and (2) they are perpendicular to the semimajor axis of the pair in the case of eccentric binaries. For a given mass ratio and eccentricity, the magnitude of these three effects is a function of orbital separation and stellar final velocity. Energetic three-body interactions eject stars in the direction of maximum black hole orbital speed, generating a larger anisotropy in higher velocity stars, and a positive z-component of the stellar angular momentum. For small binary separations, the degree of anisotropy of the ejected stars is reduced, as, in order to generate a kick above a given V, the three-body interaction need not be as strong as in the case of large separation.

4.2.1. *Latitude*

Figure 9 shows $\langle\theta^2\rangle$ as a function of binary separation, where $-\pi/2 < \theta < \pi/2$ is the latitude of ejected stars, i.e., the angle between the star velocity vector at infinity and the binary orbital plane. As an isotropic distribution would yield $\langle\theta^2\rangle = \pi^2/4 - 2 = 0.467$, values lower than this indicate that the ejected stars tend to be flattened toward the binary orbital plane. We plot results for the population of HVSs as a whole ($V > v_{esc}$) and for a subset with $V > 9v_{esc}$. Note that a value $\langle\theta^2\rangle = 0$ at large separations simply means that no stars are ejected with a velocity exceeding the given threshold, not that stars are actually scattered exactly in the binary orbital plane. Higher velocity stars are more flattened into the orbital plane, and smaller binary separations lead to a more isotropic angular distributions. At a fixed mass ratio and orbital separation, more eccentric binaries eject stars in a more isotropic fashion, while at a fixed eccentricity binaries with smaller mass ratios produce a more isotropic distribution of HVSs.

4.2.2. *Longitude*

Scattered stars typically receive a kick along the direction of maximum velocity of the MBHs. This implies that, in the case of eccentric binaries, the spatial distribution of HVSs will form a broad jet perpendicular to the semimajor axis. For small binary mass ratios, the jet tends to be one-sided, since M_1 is practically at rest and the interaction takes place close to the pericenter of M_2 (Levin 2005). For equal-mass binaries, we expect a two-sided symmetric jet instead. To quantify these effects, we have assumed that the semimajor axis coincides with the x-axis, and that the two holes orbit counterclockwise in the x-y plane. The M_2 (M_1) velocity vector at the pericenter then forms an angle $3\pi/2$ ($\pi/2$) relative to the x-axis. Let ϕ be the star longitude, i.e., the angle between the x-axis and the projection onto the orbital plane of the star velocity vector at infinity. In the case of an azimuthally symmetric distribution, $\langle\phi\rangle = \pi$, with relative dispersion $\sigma_\phi/\langle\phi\rangle = 1/\sqrt{3} = 0.58$. Figure 10 shows the mean longitude of HVSs and its dispersion for an eccentric binary with different mass ratios, as a function of a_h/a, both for the whole population of HVSs stars ($V > v_{esc}$) and for a subset with $V > 9v_{esc}$. In the case $q \ll 1$, the jet is oriented along the velocity of M_2 at pericenter, while for $q = 1$ the value $\langle\phi\rangle \simeq \pi$ does not denote axisymmetry but rather a two-sided jet oriented perpendicular to the semimajor axis (the bottom panel shows that the angular dispersion is lower than its symmetric value). HVSs are ejected more symmetrically as the binary shrinks, and, at

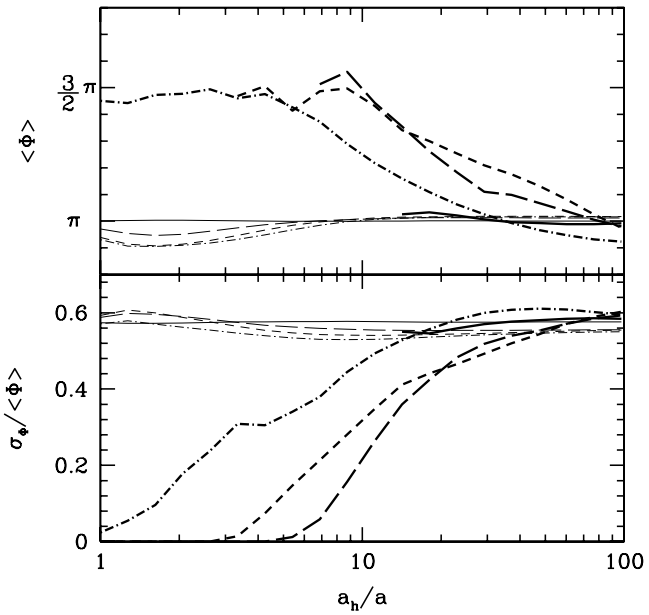

FIG. 11.—Same as Fig. 10, but for a binary with $q = 1/9$ and eccentricity $e = 0$ (*solid lines*), 0.3 (*long-dashed lines*), 0.6 (*short-dashed lines*), and 0.9 (*dot-dashed lines*). *Thin lines*: Entire population of ejected stars ($V > v_{\rm esc}$). *Thick lines:* Subset of HVSs with $V > 9v_{\rm esc}$.

any given separations, the degree of axisymmetry increases with decreasing kick velocity. The mean longitude angle as a function of eccentricity is shown in Figure 11 for a MBHB binary with $q = 1/9$. While the population of HVSs as a whole is nearly symmetric for all eccentricities regardless of binary separation, the high velocity subsample shows a clear azimuthal asymmetry for $a_h/a \lesssim 20$ that decreases with decreasing separations. MBHBs already significantly beam HVSs for $e = 0.3$; larger eccentricities produce similar values of $\langle\phi\rangle$ but at larger separations.

We note that, as well as ejection velocity, the angular properties of scattered stars also depend on the ratio V/V_c but not on the binary hardness a_h/a. This can be clearly seen in Figure 12,

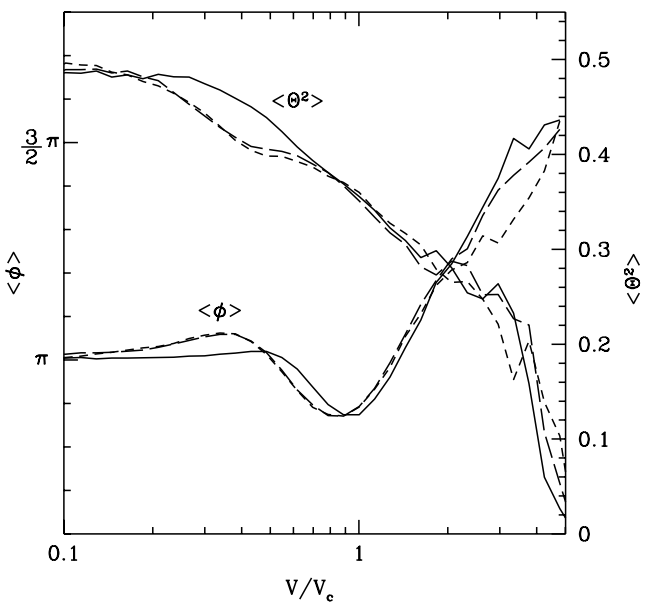

FIG. 12.—Mean values of θ^2 (*right scale axis*) and ϕ (*left scale axis*) vs. V/V_c at different binary separations: $a/a_h = 1$ (*solid lines*), $a/a_h = 0.1$ (*long-dashed lines*), and $a/a_h = 0.01$ (*short-dashed lines*). A mass ratio $q = 1/9$ and an eccentricity $e = 0.6$ are assumed.

where the mean latitude and longitude angles are plotted versus V/V_c for a binary with $q = 1/9$ and $e = 0.6$, at separations $a/a_h = 1$, 0.1, and 0.01.

5. CONCLUSIONS

We have performed full three-body scattering experiments in order to study the detailed kinematic properties of hypervelocity stars by massive black hole binaries at the center of galaxies. Ambient stars are drawn from a Maxwellian distribution unbound to the binary, and are expelled by the gravitational slingshot. Numerical orbit integration from initial conditions determined by Monte Carlo techniques provides accurate measurements of thermally averaged hardening, mass ejection, and eccentricity growth rates for MBHBs in a fixed stellar background. We have shown that binary-star interactions create a subpopulation of HVSs on nearly radial orbits, with a spatial distribution that is initially highly flattened in the inspiral plane of the MBHB, but become more isotropic with decreasing binary separation. The degree of anisotropy is smaller for unequal mass binaries and larger for stars with higher kick velocities. Eccentric MBHBs produce a more prominent tail of high-velocity stars and break axisymmetry, ejecting HVSs along a broad jet perpendicular to the semimajor axis. The jet two-sidedness decreases with increasing binary mass ratio, while the jet opening angle increases with decreasing kick velocity and orbital separation.

It is interesting to quantify the properties of the HVSs that would populate the halo of the Milky Way (MW) in the presence of a MBHB at the Galactic center. We assume that the binary total mass is $M_1 + M_2 = 3.5 \times 10^6\ M_\odot$, that Sgr A* is the most massive component M_1 of the pair, that the binary mass ratio is $q = 1/81$, and that the loss cone is always full. From our discussion in § 4.1, we expect the small mass ratio to result in a large number of HVSs. The pair is allowed to shrink from $a = a_h$ down to $a = 0.1a_h$ due to three-body interactions, within the allowed parameter space derived for a circular binary by Yu & Tremaine (2003) using a variety of observational and theoretical arguments. Figure 13 shows the quantity $d(N_{\rm HVS})/d\ln a$,

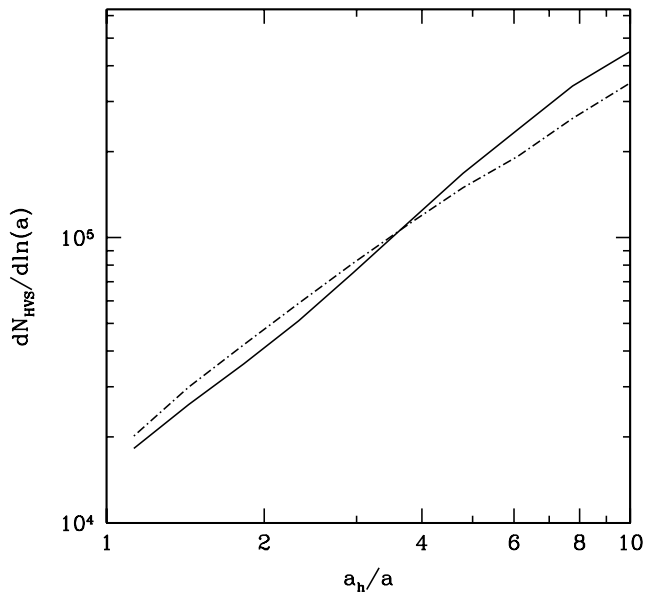

FIG. 13.—Number of HVSs escaping the MW. The binary total mass is $M_1 + M_2 = 3.5 \times 10^6\ M_\odot$, and the mass ratio is $q = M_2/M_1 = 1/81$. *Solid line*: Binary with initial eccentricity $e = 0$. *Dot-dashed line*: Binary with initial eccentricity $e = 0.9$. The total number of HVSs ejected as the pair shrinks from $a = a_h$ to $a = a_h/2$ ($a = a_h/10$) is 5×10^4 (10^6).

the number of HVSs (assuming $m_* = 1\ M_\odot$) ejected per logarithmic binary separation with $V > 1.68 v_{\rm esc}$. The adopted velocity threshold implies $V > 840$ km s^{-1} at the influence radius of the binary; it corresponds to the escape velocity from the center of the MW galaxy,[5] and translates within the MW potential to $V > 450$ km s^{-1} 10 kpc away from Sgr A*.

The curves show results for different initial eccentricities; in a self-consistent treatment of the evolution of a MBHB, we have used the results of our scattering experiments to account for the changing binary eccentricity as its orbit decays. As the orbital separation decreases from a_h to $a_h/2$, we find that the total number of HVSs is 5×10^4, for a total ejected mass of some $1.2 M_2$, independent of eccentricity; in the case of a circular binary the angular distribution of such HVSs is characterized by $\langle \theta^2 \rangle = 0.3$ and $\sigma_\phi / \langle \phi \rangle = 0.58$, while for an eccentric pair with $e = 0.9$, the latitude and azimuthal dispersions are $\langle \theta^2 \rangle = 0.37$ and $\sigma_\phi / \langle \phi \rangle = 0.6$. In the case in which the binary separation shrinks from the hardening radius down to $a = 0.1 a_h$ instead, the total number of ejected HVSs increases by a factor of 20, to 10^6; a circular binary produces an angular distribution with $\langle \theta^2 \rangle = 0.36$ and $\sigma_\phi / \langle \phi \rangle = 0.58$, while for an eccentric pair with $e = 0.9$ we find $\langle \theta^2 \rangle = 0.4$ and $\sigma_\phi / \langle \phi \rangle = 0.6$. The detection of a numerous population of HVSs in the halo of the Milky Way by the next generation of large astrometric surveys like *Gaia* may thus provide a clear signature of the history, nature, and environment of the MBH at the Galactic center.

[5] We modeled the luminous component of the MW as in Miyamoto & Nagai (1975) and the dark matter halo as in Widrow & Dubinski (2005).

We thank M. Colpi, M. Dotti, M. Rees, S. Tremaine, and A. Vecchio for discussions on the dynamics of black hole binaries. Support for this work was provided by NSF grant AST02-05738 and NASA grants NAG5-11513 and NNG04GK85G (P. M.), and by the Italian MIUR grant PRIN 2004 (A. S. and F. H.). P. M. also acknowledges support from the Alexander von Humboldt Foundation.

REFERENCES

Arnaboldi, M., Gerhard, O., Aguerri, J. A. L., Freeman, K. C., Napolitano, N. R., Okamura, S., & Yasuda, N. 2004, ApJ, 614, L33
Begelman, M. C., Blandford, R. D., & Rees, M. J. 1980, Nature, 287, 307
Brown, W. R., Geller, M. J., Kenyon, S. J., & Kurtz, M. J. 2005, ApJ, 622, L33
———. 2006a, ApJ, 640, L35
———. 2006b, ApJ, 647, 303
Dormand, J. R., & Prince, P. J. 1978, Celest. Mech., 18, 223
Edelmann, H., Napiwotzki, R., Heber, U., Christlieb, N., & Reimers, D. 2005, ApJ, 634, L181
Hairer, E., Norsett, S. P., & Wanner, G. 1993, Solving Ordinary Differential Equations, I. Nonstiff Problems (Berlin: Springer)
Haring, N., & Rix, H. W. 2004, ApJ, 604, L89
Hills, J. G. 1983, AJ, 88, 1269
———. 1988, Nature, 331, 687
Hirsch, H. A., Heber, U., O'Toole, S. J., & Bresolin, F. 2005, A&A, 444, L61
Holley-Bockelmann, K., Sigurdsson, S., Mihos, J. C., Feldmeier, J. J., Ciardullo, R., & McBride, C. 2005, ApJ, submitted (astro-ph/0512344)
Hut, P., & Bahcall, N. 1983, ApJ, 268, 319
Kazantzidis, S., et al. 2005, ApJ, 623, L67
Levin, J. 2005, preprint (astro-ph/0508193)
Magorrian, J., et al. 1998, AJ, 115, 2285
Mikkola, S., & Valtonen, M. J. 1992, MNRAS, 259, 115
Miyamoto, M., & Nagai, R. 1975, PASJ, 27, 533
Quinlan, G. D. 1996, NewA, 1, 35 (Q96)
Saslaw, W. C., Valtonen, M. J., & Aarseth, S. J. 1974, ApJ, 190, 253
Valtonen, M. J., & Aarseth, S. J. 1977, RevMexAA, 3, 163
Volonteri, M., Haardt, F., & Madau, P. 2003, ApJ, 582, 559
Widrow, L. M., & Dubinski, J. 2005, ApJ, 631, 838
Yu, Q., & Tremaine, S. 2003, ApJ, 599, 1129
Zier, C., & Biermann, P. L. 2001, A&A, 377, 23